



A Numerical Simulation of the Flow in a Diffusing S-Duct Inlet

Lifen Zhang & Zhenxia Liu

School of Power and Energy, Northwestern Polytechnical University

Xi'an 710072, China

Jian Jiang

Chinese Flight Test Establishment, Xi'an 710089, China

Abstract

A numerical simulation of the flow inside a diffusing S-duct inlet is conducted. The primary discussion herein focuses on flow analysis and development of secondary flow in the S-duct diffuser inlet. Full three-dimensional Navier-Stokes equations are solved and SST turbulence model is employed. Numerical results, including surface static pressure, total pressure recovery at exit, are compared with experiment. And fairly good agreement is apparent. Total performance, such as average total pressure recovery and distortion, is agreed well with the experiment. Shock waves in outer flow, pressure recovery and distortion at the exit are also discussed.

1. Introduction

S-duct inlet has been widely used for military and commercial aircraft, such as F-16, F-18 and Boeing 727. Inlet should decelerate the flow to the desired velocity while maintaining high total pressure recovery and flow uniformity. But in S-duct inlet two bends give rise to streamline curvature. The streamline curvature results in cross-stream pressure gradients which can produce significant secondary flows. Increasing cross-sectional area can lead to adverse pressure gradients. All of mentioned above increase risk of unacceptable inlet performance. So understanding flow in S-duct inlet is very important in inlet design process. (S.R. Wellborn, B.A. Reichert, T.H. Okiishi, 1992; B.A. Reichert, B.J. Wendt, 1993; G.J. Harloff, B.A. Reichert, S.R. Wellborn, 1992)

Usually, performance of S-duct inlet is determined by wind tunnel testing with expensive cost. But since the late 1960's, Computational Fluid Dynamics has been under continuous and wide-spread development. From 1990's, the CFD method has been developed to aid the design and analyze of aircraft propulsion component and system (G.J. Harloff, B.A. Reichert, S.R. Wellborn, 1992).

The purpose of the present study is to predict flow in a rectangular-to-circular S-duct inlet using a full Navier-Stokes equations and two-equation SST turbulence model, and analyze flow and development of secondary flow. Shock waves in outer flow, pressure recovery contour and distortion at exit are also discussed. A careful comparison of numerical predictions with experiment is necessary to establish and improve the numerical accuracy. In this paper, surface pressure, total pressure recovery and total performance are compared with experiment.

2. S-duct inlet and Numerical methods

The inlet configuration in this paper is a external compression, overhead three ramp and rectangular-to-circular designs, as shown in Fig.1. First ramp is fixed, second is removable, and the third is slaved. In order to eliminate boundary layer, there are thousands of small holes which diameter is just several millimeter in second and third ramp. The computed model is full scale, containing airframe and boundary layer diverter. Reported test is conducted with incoming Mach number of 1.2, flight altitude of 14km and zero degree angle of attack.

All solid surfaces are treated viscously and the entire flow is assumed fully turbulent. Freestream pressure is assumed at the external outflow boundary located approximately 3.5 vehicle lengths. The most difficult boundary condition is the exit of the diffuser. In this paper, static pressure at exit is estimated based on test data. In order to reduce the influence of the exit, diffuser is extended approximately 0.2 inlet lengths, pictured in Fig.2. Due to no accurate static pressure at the exit, some error is brought into the computational domain.

Full three-dimensional Reynolds-averaged Navier-Stokes equations in strong conservation form are used for computation. Two-equation SST turbulence model is employed. It has been found to be very robust and stable for a variety of flow conditions, and it solves equations for \mathcal{K} and ω in the inner region of the boundary layer and gradually changes to the high Reynolds number $\mathcal{K}-\varepsilon$ model away from the wall (F.R. Menter, 1993). Grid generation uses hybrid grid which includes tetrahedron and prism. Total number is approximately 0.5 million.

3. Results and discussion

Predicted surface static pressure and pressure recovery at exit are compared with experiment to insure accuracy of the computation. There are 15 pressure probes along the inlet surface. Surface static pressure is presented as pressure coefficients defined by Eq.1.

$$C_p = \frac{P - P_\infty}{q_\infty} \quad (1)$$

Where, P_∞ is the free stream static pressure, and q_∞ is the free stream dynamic pressure.

Numerical and experimental pressure coefficients are shown in Fig.3. Good agreement is apparent. From the picture, we can see along the inlet surface, pressure has a trend of increasing. That because velocity should be decelerated and pressure should be enhanced in diffuser.

Fig.4 displays comparison of numerical and experimental pressure recovery at exit. Probes of 21 to 24 have some disagreement between numerical and experimental. The agreement of other probes is fairly good.

Fig.5 displays Mach number along the S-duct centerline. From this picture two shock waves are observed in outer flow. The first is around airframe head, and flow is decelerated to sonic. The second is on the top lip, this shock wave is weaker than the first one. After the secondary shock wave, airflow is subsonic, and flow into S-duct inlet. Inside the inlet, the velocity is lower near the top of the surface, round the second bend, the mach number is 0.2. Near the bottom, the velocity is comparatively high. Before the second bend, the mach number reach 0.7, after the second bend, the mach number is 0.6. The high velocity at bottom mix low velocity at top along the inlet. When the flow reaches the exit, the mach number is about 0.4.

To better observe flow in the S-duct inlet, total pressure recovery in six cross-stream planes of the S-duct is presented in fig.6. In the first plane, the high total pressure is in the center and bottom, the highest value is 0.98, and the low total pressure is concentrated on the top, the lowest value is 0.79. As the flow progress downstream, the low total pressure flow develop from top to the center, and the high momentum flow is pushed to two sides. In this process, high and low momentum flow mix, and in the sixth plane, the high total pressure is around the center, and the highest value is 0.98. Area of the highest value becomes small. The low total pressure is in the center, and the lowest value is 0.89. The reason inducing the change of the total pressure is the development of secondary flow as shown in Fig.7. The curvature of the S-duct inlet's centerline gives rise to streamline curvature, which results in a cross-stream static pressure gradient initiating fluid motion within the boundary layer toward the inside of the inlet bend. In the first bend, due to the duct's curvature, a centrifugal force is produced. And pressure of outside bend is higher than inside bend, a pressure gradient is induced. In order to balance the centrifugal force, fluid has a trend to be pushed to the inside of the duct. Due to its slower velocity, the boundary layer is more sensitive to this pressure gradient. The balance of the forces on it will migrate it along the walls towards the inside of the bend more readily than the core flow. This accumulation of boundary layer fluid at the top of the bend would try to replace and push fluid already there away from the wall toward the center of the bend, thus producing lift-off effect (A.J. Anabtawi, R.F. Blackwelder, P.B.S. Lissaman, R.H. Liebeck,1999; S.E. Tournier, J.D. Paduano, D. Pagan,2005). In the second bend, curvature opposite to the first one, and the direction of the secondary flow reverse. However, secondary flow caused by first bend is very strong and no cancellation effect take place (A.J. Anabtawi, R.F. Blackwelder, P.B.S. Lissaman, R.H. Liebeck,1999). Hence, the boundary layer fluid continues to accumulate near the top of the inlet. The top is low momentum flow, secondary flow reversal should firstly occur here, so a pair of vortices comes into being. The second bend also induces a pair of vortices, although it is weak and small, as pictured in Fig.8.

The numerical results of secondary flow at exit are shown in Fig.8. At the top of the exit, a pair of vortices is observed evidently. At the two sides below, a small pair of vortices is also observed but not very distinctly.

Total pressure recovery contour is displayed in Fig.9. High total pressure is around center, and low total pressure is in the center. That results from the naturally occurring vortices convecting low-momentum fluid away from walls to center. The largest value is 0.98, the average value is 0.932, and the experimental average value is 0.936. So the total performance is very good agreement with experiment.

Distortion descriptor of IDC_{max} is used to estimate the exit distortion. It defines as follows,

$$IDC_i = \frac{P_{i,avg} - P_{i,min}}{P_{face,avg}} \quad i=1 \text{ to } 5;$$

$$\overline{IDC}_j = \frac{IDC_j + IDC_{j+1}}{2} \quad j=1 \text{ to } 4;$$

$$IDC_{\max} = \text{Max}(\overline{IDC}_j) \quad j=1 \text{ to } 4;$$

The experimental value is 0.0570, and the numerical value is 0.0511. So the numerical result is agreed well with experimental.

4. Summary

There are two shock waves in outer flow. One is around airframe, the other is on the top lip. The shock waves decelerate velocity and increase pressure. In the S-duct inlet, pressure-driven secondary flow which is caused by curvature results in two pairs of vortices. One pair caused by first bend are large, the other caused by second bend are small and weak. These vortices convect the low momentum fluid of the boundary layer towards the center of the duct, degrading both the uniformity and total pressure recovery. Total performance, such as average total pressure recovery and distortion descriptor IDC, is agreed very well with experiment. And some details, including surface static pressure and total pressure recovery at exit, have fairly good agreement with experiment.

References

A.J. Anabtawi, R.F. Blackwelder, P.B.S. Lissaman, R.H. Liebeck, An experimental investigation of boundary layer ingestion in a diffusing S-duct with and without passive flow control. AIAA 99-2110.

B.A.Reichert, B.J.Wendt, An experimental investigation of S-duct flow control using arrays of low-profile vortex generators, AIAA 93-0018.

F.R. Menter, Zonal two equation $\kappa - \omega$ turbulence models for aerodynamic flows. AIAA 93-2906.

G.J. Harloff, B.A. Reichert, S.R. Wellborn, Navier-Stokes analysis and experimental data comparison of compressible flow in a diffusing S-duct. AIAA 92-2699.

S.E. Tournier, J.D. Paduano, D. Pagan, Flow analysis and control in a transonic inlet. AIAA 2005-4734.

S.R.Wellborn, B.A.Reichert, T.H.Okiishi, An experimental investigation of the flow in a diffusing S-duct, AIAA 92-3622.



Figure 1. Sketch of the S-duct inlet

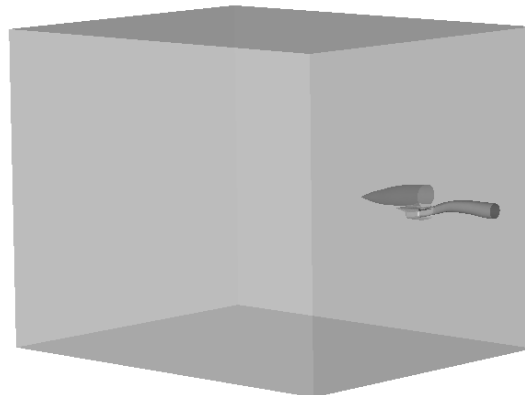


Figure 2. Computational domain

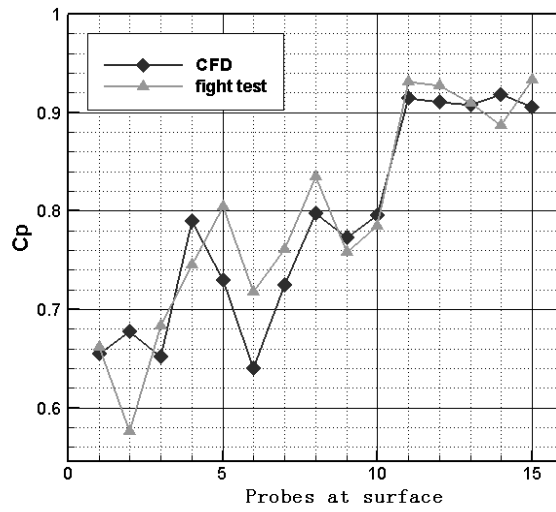


Figure 3. Surface static pressure coefficient

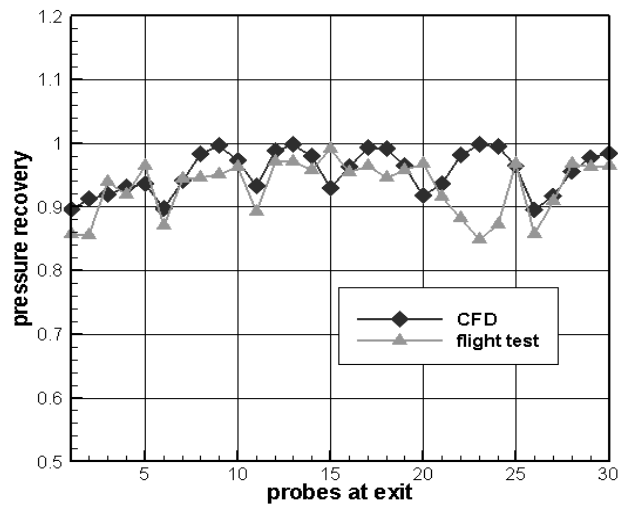


Figure 4. Total pressure recovery at exit

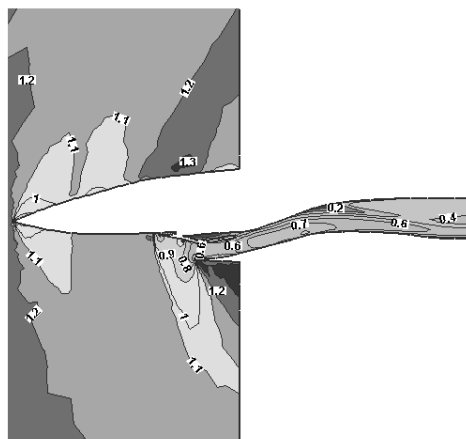


Figure 5. Mach number along the S-duct centerline

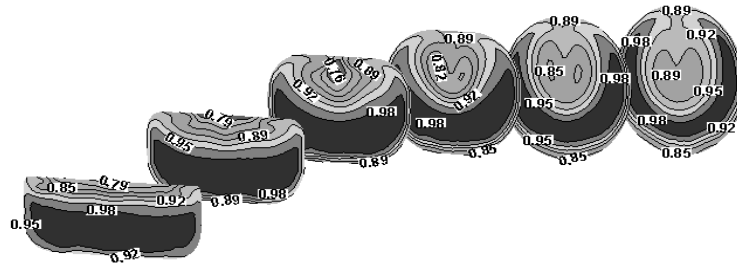


Figure 6. Total pressure recovery in six cross-stream planes

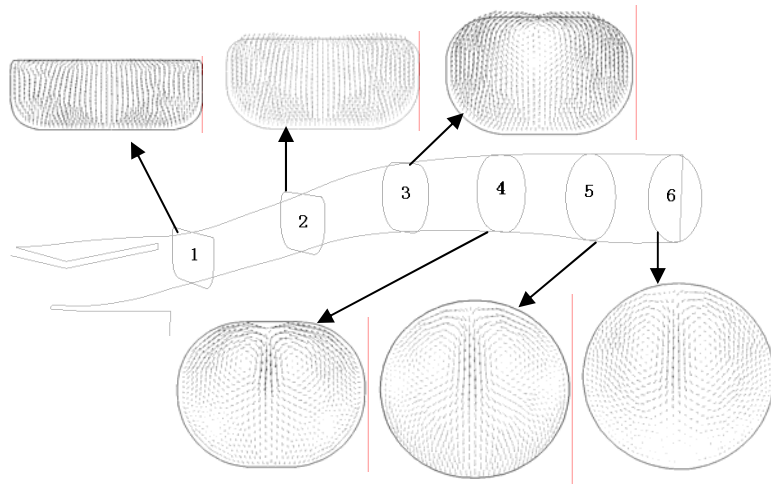


Figure 7. Secondary flow in six cross-stream planes

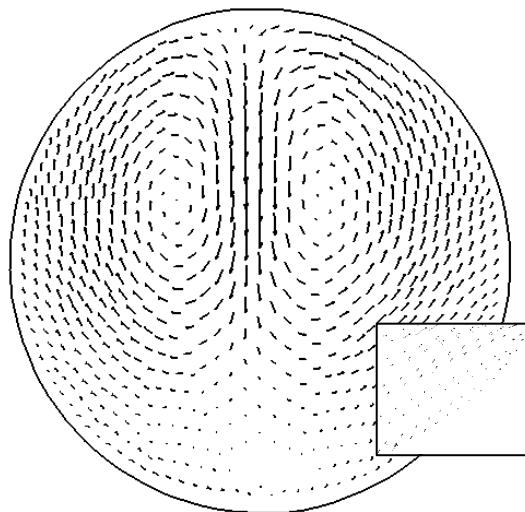


Figure 8. Secondary flow at exit

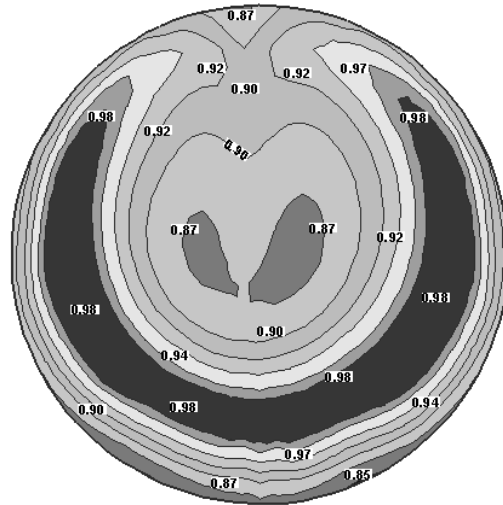


Figure 9. Total pressure recovery at exit